Evaluating the correspondence between face-, scene-, and object-selectivity and retinotopic organization within lateral occipitotemporal cortex

Edward H. Silson Laboratory of Brain and Cognition, National Institute of Mental Health, National Institutes of Health, Bethesda, MD, USA

Iris I. A. Groen Laboratory of Brain and Cognition, National Institute of Mental Health, National Institutes of Health, Bethesda, MD, USA

Dwight J. Kravitz Department of Psychology, George Washington University, Washington, DC, USA

Chris I. Baker Laboratory of Brain and Cognition, National Institute of Mental Health, National Institutes of Health, Bethesda, MD, USA

The organization of human lateral occipitotemporal cortex (lOTC) has been characterized largely according to two distinct principles: retinotopy and category-selectivity. Whereas category-selective regions were originally thought to exist beyond retinotopic maps, recent evidence highlights overlap. Here, we combined detailed mapping of retinotopy, using population receptive fields (pRF), and category-selectivity to examine and contrast the retinotopic profiles of scene- (occipital place area, OPA), face- (occipital face area, OFA) and object- (lateral occipital cortex, LO) selective regions of lOTC. We observe striking differences in the relationship each region has to underlying retinotopy. Whereas OPA overlapped multiple retinotopic maps (including V3A, V3B, LO1, and LO2), and LO overlapped two maps (LO1 and LO2), OFA overlapped almost none. There appears no simple consistent relationship between category-selectivity and retinotopic maps, meaning category-selective regions are not constrained spatially to retinotopic map borders consistently. The multiple maps that overlap OPA suggests it is likely not appropriate to conceptualize it as a single scene-selective region, whereas the inconsistency in any systematic map overlapping OFA suggests it may constitute a more uniform area. Beyond their relationship to retinotopy, all three regions evidenced strongly retinotopic voxels, with pRFs exhibiting a significant bias towards the contralateral lower visual field, despite differences in pRF size, contributing to an emerging literature suggesting this bias is present across much of lOTC. Taken together, these results suggest that whereas category-selective regions are not constrained to consistently contain ordered retinotopic maps, they nonetheless likely inherit retinotopic characteristics of the maps from which they draw information.

Introduction

The functional properties of the lateral surface of human occipitotemporal cortex (lOTC) have been characterized historically according to two main organizing principles: *retinotopy*—the spatial mapping of the retina across the cortical surface (DeYoe et al., 1996; Engel et al., 1994; Sereno et al., 1995), and *category-selectivity*—*the* observation that certain cortical regions exhibit selective responses to stimuli from particular categories (Epstein & Kanwisher, 1998; Kanwisher, McDermott, & Chun, 1997; Zeki, Kennard, Watson, Lueck, & Frackowiak, 1991). Multiple maps of the visual field tile the surface of lOTC (Wandell, Dumoulin, & Brewer, 2007), extending dorsally and anteriorly from primary visual cortex (V1) into the intraparietal sulcus

Citation: Silson, E. H., Groen, I. I. A., Kravitz, D. J., & Baker, C. I. (2016). Evaluating the correspondence between face-, scene-, and object-selectivity and retinotopic organization within lateral occipitotemporal cortex. *Journal of Vision*, *16*(6):14, 1–21, doi:10.1167/16.6.14.

doi: 10.1167/16.6.14 Received December 7, 2015; published April 22, 2016 ISSN 1534-7362

(Swisher et al., 2009). lOTC also contains regions that exhibit selective responses to stimuli from different categories, including faces, bodies, objects and scenes (Downing, Jiang, Shuman, & Kanwisher, 2001; Hasson, Harel, Levy, & Malach, 2003; Malach et al., 1995; Nakamura et al., 2000; Silvanto, Schwarzkopf, Gilaie-Dotan, & Rees, 2010). Although historically these organizing principles have been considered largely independently, more recent neuroimaging (Amano, Wandell, & Dumoulin, 2009; Golomb & Kanwisher, 2012; Kravitz, Kriegeskorte, & Baker, 2010; Larsson & Heeger, 2006; Sayres & Grill-Spector, 2008; Silson, Chan, Reynolds, Kravitz, & Baker, 2015; Weiner & Grill-Spector, 2011) and neurostimulation (Silson et al., 2013) studies have demonstrated that, in certain regions of lOTC, these principles are not mutually exclusive and indeed can coexist at the same location (Kravitz, Vinson, & Baker, 2008; Kravitz, Saleem, Baker, Ungerleider, & Mishkin, 2013). Here, we focus principally on scene-selective occipital place area (OPA, also referred to as transverse occipital sulcus, or TOS, (Bettencourt & Xu, 2012; Dilks, Julian, Paunov, & Kanwisher, 2013; Nasr et al., 2011), face-selective occipital face area, OFA (Haxby, Hoffman, & Gobbini, 2000; Pitcher, Walsh, & Duchaine, 2011; Silvanto et al., 2010), and object-selective lateral occipital cortex, LO (Malach et al., 1995), and ask how do these category-selective regions relate to the retinotopic maps that also tile the surface of lOTC? A number of previous reports have endeavored to map the relationship between retinotopy and category-selectivity in lOTC. For instance, different frameworks have been proposed to describe the overlap between body-selective extrastriate body area (EBA – Downing et al., 2001; Taylor et al., 2007) and retinotopic divisions of motion-selective area V5/MT (Ferri, Chiarelli, Merla, Gallese, & Costantini, 2013; Weiner & Grill-Spector, 2011). Object-selective LO (Malach et al., 1995) has been shown to overlap partially with visual field maps LO1 and LO2 (Larsson & Heeger, 2006; Sayres & Grill-Spector, 2008). In addition, a study (Nasr et al., 2011) exploring scene-selective regions in humans and macaque highlighted that in human, OPA was generally situated anterior and ventral of V3A, extending inferiorly from V7 (IPS0) through V3B and LO1. Although this report was the first to relate the location of OPA to retinotopic maps, the analysis did not provide a quantification of this relationship, and moreover, was limited to a relatively small number of participants. Further, we recently demonstrated a significant retinotopic bias for the contralateral lower visual field within OPA (Silson et al., 2015). In contrast to this previous work considering object-, body-, and scene-selective regions of lOTC, the relationship between face-selective OFA and visual field maps has received much less attention.

Here, we utilized detailed mapping of both population receptive fields (pRF) and category-selectivity to quantify the spatial relationship between OPA, OFA, LO, and lOTC visual field maps. Our data highlight that whereas OPA exhibits considerable overlap with multiple maps, LO overlaps fewer, and OFA exhibits almost no overlap. Despite contrasting relationships to underlying retinotopy, all regions evidence a significant bias towards the contralateral lower visual field (see also Silson et al., 2015). OFA and LO also contain significantly smaller pRFs and much denser representations of the fovea than OPA. Taken together, despite much overlap, there appears no simple consistent relationship between retinotopy and category-selectivity throughout lOTC. Moreover, although category-selective regions appear not to be consistently constrained to particular retinotopic maps, they likely inherit retinotopic characteristics from the maps they either encompass, in the case of OPA and LO, or are adjacent to, in the case of OFA.

Materials and methods

Participants

Sixteen participants (nine male, seven female; mean age = 31 years old) participated in the fMRI experiments. All participants had normal or corrected-to-normal vision and gave written informed consent. The National Institutes of Health Institutional Review Board approved the consent and protocol. This work was supported by the Intramural Research program of the National Institutes of Health—National Institute of Mental Health Clinical Study Protocol 93-M-0170, NCT00001360.

fMRI scanning parameters

Participants were scanned on either a research-dedicated GE 3 Tesla Sigma scanner or a research-dedicated Siemens 7 Tesla Magnetom scanner in the Clinical Research Centre on the National Institutes of Health campus (Bethesda, MD).

In all scans and across scanners, oblique slices were oriented approximately parallel to the base of the temporal lobe and extended posteriorly through all of visual cortex. All participants completed at least eight runs of pRF mapping as well as two runs of an additional category-selective functional localizer. In a separate session a subset of participants completed either additional category-selective functional localizer scans ($n = 5$) or checkerboard mapping pRF sessions ($n = 7$).

3T scanning parameters

Partial volumes of the occipital and temporal cortices were acquired using an eight-channel head coil

(21 slices; 2 × 2 × 2 mm; 10% interslice gap; TR 2s; TE 30 ms; matrix size, 96 × 96; FOV 192 mm), during pRF mapping sessions and initial category-selective localization.

7T scanning parameters

Partial volumes of the occipital and temporal cortices were acquired using a thirty-two-channel head coil (42 slices; 1.2 × 1.2 × 1.2 mm; 10% interslice gap; TR 2s, TE 27 ms; matrix size, 170 × 170; FOV 192 mm) during pRF mapping sessions and initial category-selective localization, with additional localization scans occurring at a slightly larger voxel volume (47 slices; 1.6 × 1.6 × 1.6 mm; 10% interslice gap; TR 2s, TE 27 ms; matrix size, 126 × 126; FOV 192 mm).

Visual Stimuli and Tasks

Population receptive field mapping

During the primary pRF mapping sessions a bar aperture traversed gradually through the visual field, while revealing randomly selected scene fragments from a total of 90 color images. During each 36-s sweep, the aperture took 18 evenly spaced steps every 2 s (1TR) to traverse the entire screen. During each bar position five scene fragments were displayed in rapid succession (400 ms per image). Across the 18 aperture positions all 90 possible scene images were displayed once. A total of eight sweeps were made during each run (four orientations, two directions). Specifically, the bar aperture progressed in the following order for all (eight) runs: Left to Right, Bottom Right to Top Left, Top to Bottom, Bottom Left to Top Right, Right to Left, Top Left to Bottom Right, Bottom to Top, and Top Right to Bottom Left. The bar stimuli covered a circular aperture (20° diameter 7T, 15° diameter 3T). Participants performed a color detection task at fixation, indicating via button press when the white fixation dot changed to red. Color fixation changes occurred semirandomly, with approximately two color changes per sweep (Silson et al., 2015). Seven participants also completed checkerboard mapping sessions (eight runs), in which the bar aperture revealed a 100% contrast reversing checkerboard (8 Hz). The spatial and temporal parameters of the bar aperture were identical to that during primary pRF mapping runs.

Category-selective functional localizers

All participants initially completed two scans in order to localize scene- and face-selective areas of lOTC. These scans employed an on/off design (scenes/faces) with alternating 16-s blocks of 20 stimuli (5° × 5°) presented while participants performed a one-back task. Eight participants also completed two object-selective localizer runs, whereby the same on/off design was employed, but images alternated between objects and scrambled versions of the objects. Additionally five participants completed four localizer scans employing a multiblocked design in order to identify these same regions using different functional contrasts. In these sessions, images from eight categories including faces, buildings, scenes (manmade/natural, open/closed), and man-made and natural objects, were presented in 16-s blocks with an 8-s blank fixation period separating blocks. Each category was presented twice per run, and the order of presentation was counterbalanced across participants and runs.

fMRI data preprocessing

All data were analyzed using the Analysis of Functional NeuroImages (AFNI) software package (Cox, 1996, http://afni.nimh.nih.gov/afni). Prior to statistical and pRF analyses, all images for each participant were motion corrected to the first image of the first run, after removal of the appropriate "dummy" volumes (eight) to allow stabilization of the magnetic field. Postmotion-correction data were smoothed with a 2-mm full-width at half-maximum Gaussian kernel for both 3T and 7T localizer runs only.

Localizer analysis

To identify category-selective regions of interest (ROI), significance maps of the brain were computed in each participant by performing a correlation analysis between the assumed hemodynamic response function and the activation time courses thresholded at $p < 0.0001$ (uncorrected). Only contiguous clusters of voxels (>25) exceeding this threshold were defined as category-selective. The anatomical locations of these clusters were inspected in order to define ROIs consistently with previously published work (Kravitz et al., 2010; Sayres & Grill-Spector, 2008; Schwarzlose et al., 2008; Silson et al., 2015). The additional multiblock localizer runs were analyzed by conducting a standard general linear model implemented in AFNI. Specifically, a response model was built by convolving a standard gamma function with a 16 s square wave for each condition and compared against the activation time courses using Generalized Least Squares (GLSQ) regression. Motion parameters and four polynomials accounting for slow drifts were included as regressors of no interest. To derive the response magnitude per category, t tests were performed between the category-specific beta estimates and baseline.

pRF mapping analysis

Both primary and additional checkerboard pRF analyses of unsmoothed data were conducted in AFNI, using a pRF implementation for the AFNI distribution (Silson et al., 2015), based broadly on previous pRF implementations (Dumoulin & Wandell, 2008; Larsson & Heeger, 2006). For every voxel in the brain, the model estimates initially the center of the pRF on an X, Y grid with 200 samples across both the height and the width of the field of view. For each point in the grid, sigma (pRF size), values are sampled at the same resolution, but over a default range of 0 to half the field of view (sampled at 100 even intervals). These default parameters result in 4 million possible pRFs (X, Y location and sigma). Given the position of the stimulus in the visual field at every TR, the estimated time series for a receptive field of a given location (X, Y) and size (sigma) can be modeled. The model then makes use of a 2-D stimulus time series, which contains binary masks of the stimulus location at each TR and a convolution with a standard hemodynamic response function to produce 4 million predicted time series. Both Simplex and Powell optimization algorithms are utilized to find the best time series/parameter sets (X, Y, and sigma) by minimizing the least squares error of the predicted time series measured against the acquired time series in each voxel: the model outputs for each voxel, *the* X, Y location represents the center of the receptive field; sigma, which represents the diameter (size) of the receptive field; and R^2, which corresponds to the explained variance of the fit and can be used to statistically threshold these data.

Delineation of visual field maps

To identify visual field maps in individual participants, the representations of polar angle and eccentricity were visualized on surface reconstructions of both hemispheres and inspected. Surface reconstructions of the gray and white matter boundary of individual participant hemispheres were made using the Freesurfer4 autorecon script http://surfer.nmr.mgh.harvard.edu/). Retinotopically organized maps were visible and present in all tested hemispheres. Notwithstanding subtle interparticipant variability, the main features of the maps, in particular the reversals in visual field representation at the vertical and horizontal meridians, were consistent across participants. In accordance with previous reports (DeYoe et al., 1996; Engel et al., 1994; Larsson & Heeger, 2006; Sereno et al., 1995; Wandell et al., 2007), retinotopic visual field maps were delineated using the following criteria: (a) the polar angle representations displayed reversals. That is, the representations of polar angle in neighboring visual areas were mirror reversals of one another, with a reversal in the representation along their shared boundary; (b) the polar angle and eccentricity components within each visual area were organized largely orthogonal to one another. The following visual field maps were identified in each hemisphere and participant (V1, V2d, V2v, V3d, V3v, hV4, V3A, V3B, V7 (IPS0), LO1, and LO2). In order to demonstrate the visual field coverage in our retinotopic maps, we utilized data from seven participants who also completed independent checkerboard mapping sessions. Visual field map boundary definitions, using the criteria described above, were made on the basis of this checkerboard mapping data. The resulting retinotopic boundaries were then applied to data obtained during our primary pRF sessions in the same participants. This independent sampling avoids circular analyses, which can arise when one defines the boundaries of visual field maps and subsequently plots visual field coverage from the same region and data—the extent of visual field coverage will reflect directly where the boundaries of a given visual area are drawn in that specific dataset.

Defining the venous eclipse and overlap with OFA

In each participant, we identified the venous eclipse following published guidelines (Winawer et al., 2010). Initially, we calculated the mean BOLD signal across each pRF run and then averaged across all runs and normalized the values between 0 and 1. To arrive at a threshold for determining a venous eclipse ROI we calculated the distribution of normalized BOLD values in each hemisphere separately and averaged across participants. These distributions revealed a bimodal structure in both hemispheres, with the peak around zero taken as reflecting the influence of large vessels including the dural sinus (Figure S1). We selected the lowest point between the two peaks in each distribution as our threshold for the venous eclipse. To calculate the overlap with OFA we calculated the proportion of nodes in OFA that had a normalized BOLD value less than or equal to our threshold.

Results

Here, using a combination of detailed pRF and category-selective mapping, we evaluate and quantify the spatial relationship between scene-, face-, and object-selective regions of lOTC and maps of the visual field, which tile this cortical surface. Further, we provide a detailed characterization and comparison of receptive fields in OPA, OFA, and LO.

Correspondence between OPA, OFA, LO and retinotopic maps within lOTC

In each participant ($n = 16$), and consistent with previous definitions (Kravitz et al., 2011; Nasr et al., 2011; Silson et al., 2015), OPA was defined as a scene-selective region (scenes > faces, $p < 0.0001$ uncorrected) located on the surface of lOTC, with OFA, defined by the opposite contrast, occupying a more ventral region of lOTC. In a smaller sample of participants ($n = 8$) we also identified LO using the contrast (objects > scrambled objects, $p < 0.0001$ uncorrected). Consistent with prior work (Larsson & Heeger, 2006; Malach et al., 1995; Sayres & Grill-Spector, 2008), LO was located ventral of OPA and in close proximity to OFA, albeit slightly more posterior.

The representation of polar angle and its relationship to the lateral visual field maps can be seen on a spherical representation of the right hemisphere of a representative participant (Figure 1A), along with the representation of eccentricity (Figure 1B). The locations of OPA and OFA relative to these retinotopic map boundaries is demonstrated in Figure 1C, with the location of LO shown in Figure 1D. OPA can be seen to overlap with multiple maps, with more pronounced overlap occurring with V3B and LO2. Of note, a portion of OPA also falls slightly anterior of V3B/LO2 that may include visual areas TO1 and TO2 (Amano et al., 2009), although we were unable to resolve these maps reliably across participants. In strong contrast, OFA exhibits a vanishingly small degree of overlap with any defined lateral visual field maps, situated typically ventral and slightly anterior of the inferior boundaries of these maps (Figure 1C). From the example shown in Figure 1A, it could potentially be argued that there are additional maps extending dorsally from V4 and terminating with LO2/TO1. However, such representations were highly variable across participants; therefore, we restricted our retinotopic definitions to those maps identifiable in all participants and hemispheres and firmly established in the literature. LO can be seen to overlap largely with the inferior boundaries of LO1 and LO2 (Figure 1D), which correspond to the representation of the fovea in these visual field maps (Figure 1B).

In order to quantify the relationship between retinotopy and category-selectivity in these regions across participants, we performed two related analyses. Initially, we calculated the overlap (proportion of surface nodes) between OPA, OFA, LO, and lateral visual field maps in all participants bilaterally (32 hemispheres in the cases of OPA and OFA and 16 hemispheres in the case of LO). Surface nodes corresponding to the boundaries between maps were excluded from the analysis, so that overlap with our category-selective ROIs could be calculated independently for each map. The pattern of overlap with underlying maps did not differ significantly between hemispheres for any ROI (paired t test for each map $p > 0.05$, in all cases). These data are displayed as pie charts for all ROIs in Figure 2, collapsed across hemispheres. Figure 2A reveals a higher degree of overlap between OPA, and V3B and LO2, relative to the other maps. OPA showed almost no overlap (<1%) with early visual areas V1-V3d (not shown in Figure 2A), and only modest overlap with V3A, V7, and LO1. Additionally, OPA also overlapped with a region of cortex that lay anterior of our retinotopic maps, potentially corresponding to TO1/ TO2 (Amano et al., 2009; see Figure 2A). In stark contrast, OFA exhibited no overlap with our more dorsal retinotopic definitions (V3A, V3B, and V7), very little overlap with early visual areas (V1–V3d) and only slightly higher overlap with LO1 and LO2—this overlap occurring at the most inferior portions and foveal representations of these maps. Indeed, at the group level ~ 95% of OFA overlapped with regions of cortex ventral and slightly anterior of our retinotopic map boundary definitions (Figure 2B). Consistent with previous studies (Larsson & Heeger, 2006; Sayres & Grill-Spector, 2008) LO1 and LO2 exhibit a higher degree of overlap with LO than other lateral surface maps (Figure 2C), but LO also extends beyond the borders of LO1 and LO2 more anteriorly.

Calculation of percentage overlap is dependent on the threshold with which the functional regions are defined initially. Therefore, we also calculated the frequency with which the peak of scene-selectivity within OPA, face-selectivity within OFA, and object-selectivity within LO fell within the boundaries of the different maps (Figure 3). Understanding this relationship is important as the voxel of peak-selectivity is used frequently to identify the target site in many neurostimulation studies of these areas (Dilks et al., 2013; Pitcher, Charles, Devlin, Walsh, & Duchaine, 2009; Pitcher et al., 2011). Consistent with our previous analyses, we observed that the peak of scene-selectivity within OPA fell within the boundaries of V3B (10 hemispheres) and LO2 (eight hemispheres) most frequently, relative to other visual field maps (Figure 3A). The peak of scene-selectivity within OPA was never found within the boundaries of V1–V3d, and only rarely within V3A, V7, and LO1, respectively. Of note, the peak of scene-selectivity within OPA was located anterior of V3B and LO2 in six hemispheres (Figure 3A). The peak of face-selectivity in OFA, however, was found to fall outside of our lateral retinotopic map definitions in all but one hemisphere (Figure 3B). The peak of object-selectivity in LO fell within the boundaries of LO1 and LO2

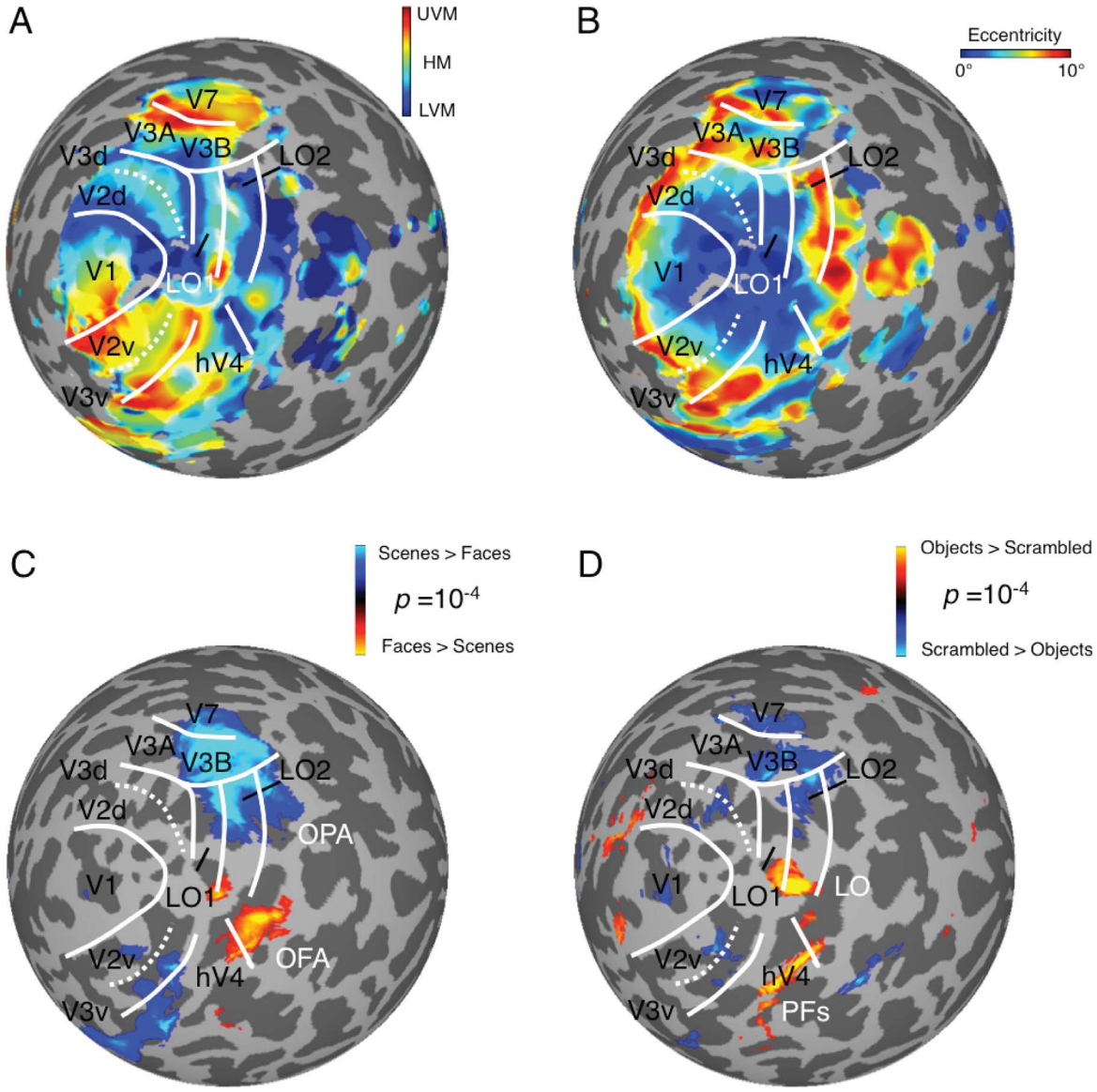

Figure 1. Correspondence between OPA, OFA, LO and lateral retinotopic maps in a representative participant. (A) Visual field maps of the right hemisphere of a representative participant displayed on a spherical surface reconstruction of the gray-white matter boundary (gyri light gray, sulci dark gray). The representation of polar angle is overlaid in false color onto this surface reconstruction. The representation of the upper vertical meridian is shown in red, with the horizontal and lower vertical meridians represented by green and blue, respectively. (B) Representation of eccentricity in the same participant can be seen to extend from the large foveal confluence (blue-0°) towards the periphery (red-10°). The boundaries of retinotopic maps defined in (A) are overlaid. (C) The location of OPA (Scenes $>$ Faces, $p < 0.0001$, uncorrected) and OFA (opposite contrast) can be seen relative to retinotopic map boundaries. OPA overlaps predominantly with visual field maps V3B and LO2, whereas OFA remains largely spatially distinct from retinotopic maps on the lateral surface. (D) The location of LO (Objects $>$ Scrambled Objects, $p < 0.0001$, uncorrected) relative to retinotopic maps. LO overlaps largely with the most inferior portions of LO1 and LO2.

equally (3 hemispheres), but outside of these and any other retinotopically defined region in all remaining hemispheres. Taken together, our analyses demonstrate that whereas OPA encompasses multiple maps, in particular V3B and LO2, LO, overlaps largely with LO1 and LO2 only, and OFA appears largely spatially distinct from retinotopically mapped regions of lOTC.

Retinotopically driven responses within OFA, despite lack of consistent overlap

Whereas OPA (and to a lesser extent LO) exhibits considerable overlap with multiple retinotopic maps, OFA exhibits almost none. Given this, one might be tempted to conclude that OFA is therefore, retinotopically insensitive and lacks retinotopic organization.

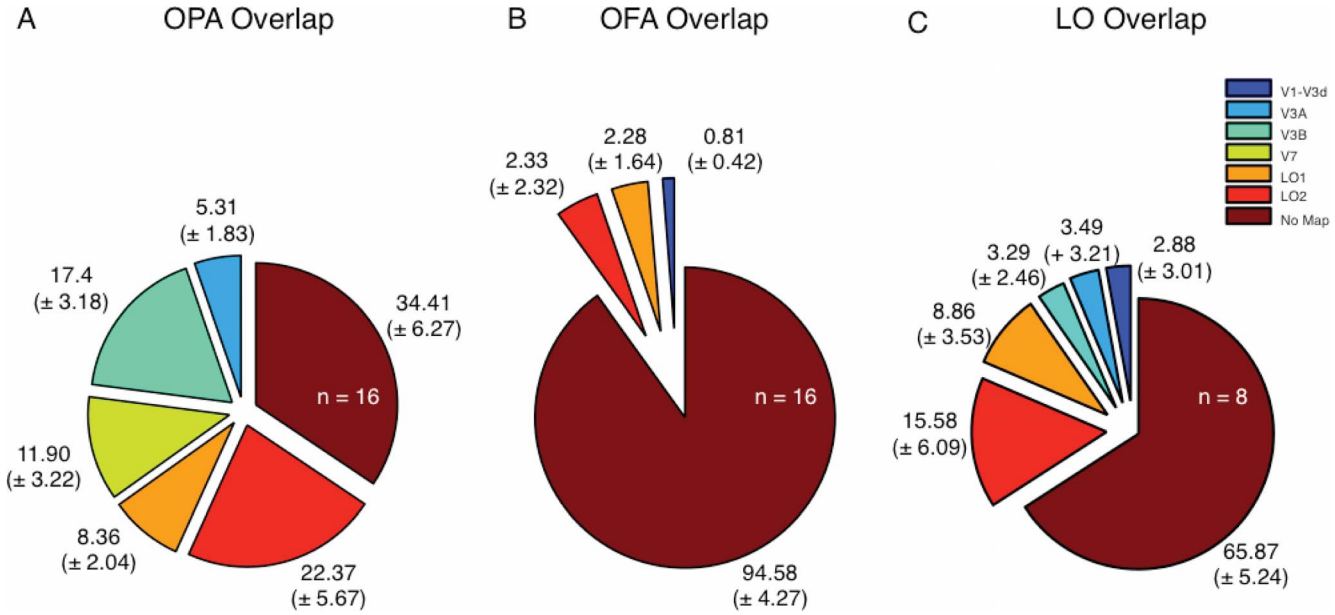

Figure 2. Quantification of spatial relationship between OPA, OFA, LO and retinotopic maps. (A) Group-average proportion of OPA surface nodes shared by lateral retinotopic maps collapsed across hemispheres. Across participants, OPA overlaps more with V3B and LO2 than with other visual field maps, although of note, more of OPA is located anterior of our retinotopic definitions (no map). Group-average proportions (± *SEM*) are plotted next to each maps corresponding wedge. Areas of cortex which showed < 5% overlap are not shown in (A). (B) Group-average proportion of OFA surface nodes shared by lateral visual field maps collapsed across hemispheres. Unlike OPA, OFA shows a vanishingly small overlap with lateral visual field maps, with the vast majority of OFA falling outside of our retinotopic definitions. (C) Group-average proportion of LO surface nodes shared by lateral visual field maps. LO overlaps LO1 and LO2 to a higher degree than other visual field maps, but also extends beyond our retinotopically mapped regions. Only maps with > 0% overlap are included as wedges.

However, we observe highly reliable retinotopically driven signals from OFA across participants, despite our primary mapping stimuli containing fragments of scenes—a stimulus which typically does not drive OFA strongly.

To illustrate this retinotopic sensitivity in OFA, and OPA and LO for comparison, we calculated the average time-course from all voxels within right OFA, OPA, and LO for each participant, and then averaged across participants (16 hemispheres for OPA and OFA, eight hemispheres for LO). Notwithstanding subtle variation in the time-courses of voxels with different pRF locations and sizes, these group-level mean time-courses highlight the overall retinotopic bias of each area at a gross level (Figure 4), revealing a number of noteworthy features.

First, for all areas, Figure 4A demonstrates clearly eight peaks of activity, which correspond to the eight sweeps our pRF mapping stimulus made through the visual field and thus through the pRF of voxels within these regions. From these group-level average time-courses, we calculated the position in the visual field corresponding to each sweeps peak (adjusted temporally to account for the lag in hemodynamic response). Figure 4B shows the region of visual space over which these bar positions overlap maximally, reflecting the position in the visual field that these regions are most sensitive to. In OFA, this region covers a small portion of the lower left quadrant of the visual field (contralateral visual field), close to, but importantly, left of the vertical meridian (vertical dashed line). In OPA, the region of maximum overlap is similarly located in the lower left quadrant, but is relatively more scattered. LO's overlap shows a striking resemblance to OFA and again occupies largely the lower left quadrant. Second, the width of each peak of activity is narrower in OFA and LO than in OPA (Figure 4A). This difference reflects the small pRF size of voxels in these regions relative to OPA. Crucially, if either OFA, OPA, or LO were insensitive to visual field position, as would be the case with a truly nonretinotopic region, such a systematic pattern of activity would be unlikely to occur.

Population receptive field profiles of OPA, OFA, and LO

Given the highly reliable retinotopically specific responses in our ROIs (Figure 4), we sought to characterize their pRF profiles in a number of ways. Initially, visual field coverage plots (Silson et al., 2015;

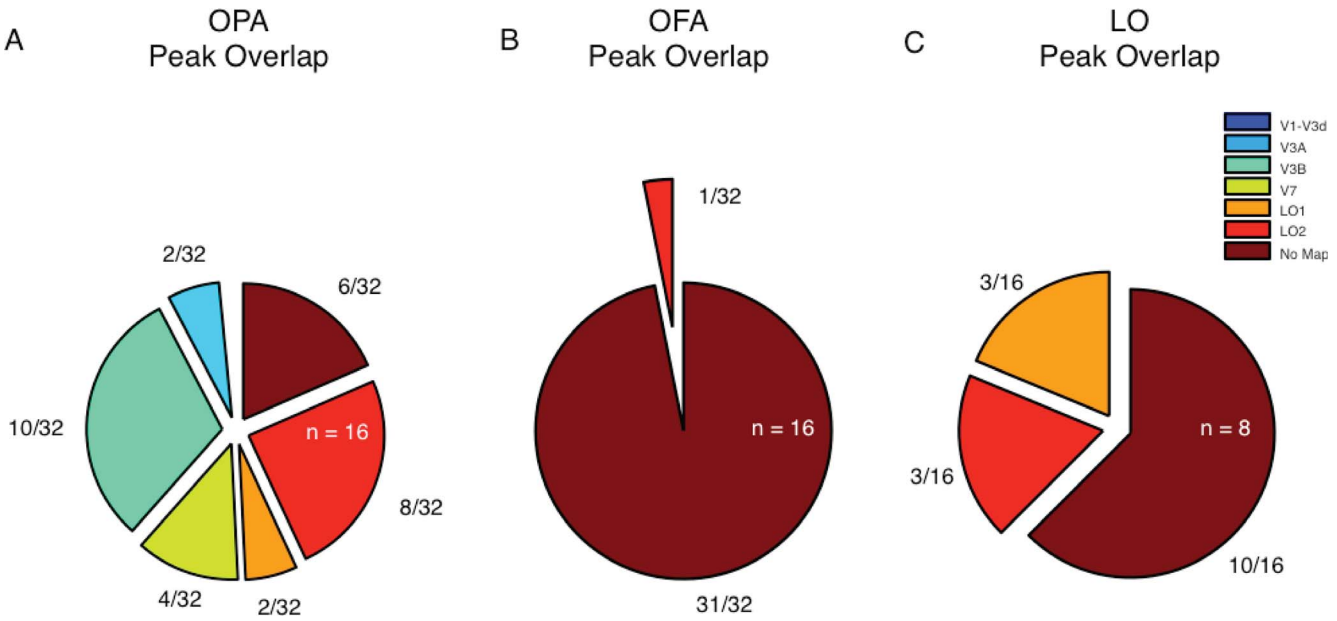

Figure 3. Frequency of peak overlap in OPA, OFA, LO and retinotopic maps. (A) Group-average frequency counts for the peak of scene-selectivity in OPA are shown, collapsed across hemispheres. Across participants, the peak of scene-selectivity within OPA falls within the boundaries of V3B and LO2 more frequently than either other visual field maps, or outside of retinotopic cortex (no map). (B) Group-average frequency counts for the peak of face-selectivity in OFA are shown, collapsed across hemispheres. Unlike OPA, the peak of face-selectivity falls within retinotopic boundaries only once. (C) Group-average frequency counts for the peak of object-selectivity in LO are shown. The peak of object-selectivity falls within LO1 and LO2 equally and beyond our map definitions in all remaining hemispheres. The frequency of overlap is plotted next to each maps corresponding wedge. Only maps with a frequency $>$ 0 are included as wedges.

Winawer et al., 2010) were computed for each participant and region (Figure 5A). At the group level, all three regions (bilaterally), exhibit a clear contralateral visual field bias, coupled with an overrepresentation of the contralateral lower visual field (Figure 5A). The representation of the visual field in OFA and LO is consistent with OPA (contralateral and lower), but extends much less into other quadrants of the visual field, reflecting both the more foveal position and smaller size of OFA and LO pRFs. The group-average proportion of pRF centers in all four quadrants of the visual field (Figure 5A) confirms the contralateral lower visual field biases present within these regions. To quantify these biases statistically, we computed (a) contralateral bias (contralateral *minus* Ipsilateral, pRF value; Figure 5B) and (b) elevation bias (Contralateral upper field *minus* contralateral lower field, pRF value; Figure 5C) measurements in each participant and ROI. These analyses confirm a significant contralateral bias (Figure 5B), coupled with a significant bias for the contralateral lower visual field (Figure 5C) in all regions, bilaterally ($p < 0.05$, in all cases, relative to zero bias). This approach mirrors our laboratory's previous method for quantifying visual field biases present in other category-selective regions of OTC (Silson et al., 2015).

Second, we examined further the pRF profiles of these regions by computing the distribution of pRF centers in the X dimension (left-right visual field position), bilaterally. We calculated, for each participant, the proportion of voxels with pRF centers that fell within one of forty linearly spaced bins spanning the width of our field of view. Group-average raw distributions (Figure 6A) and cumulative distribution functions (CDF) (Figure 6B) quantify the contralateral bias in left and right OFA, respectively. Indeed, in both cases distributions are skewed clearly in the direction of the contralateral visual field (left OFA = right visual field; right OFA = left visual field). Such a contralateral bias is consistent with previous findings of a contralateral preference for preferred categories within lOTC (Hemond et al., 2007; Kay et al., 2015; Niemeier et al., 2004), but extends them to quantify this contralateral bias in terms of the pRF properties of OFA voxels. In addition, this contralateral bias is consistent with that reported previously for OPA (Silson et al., 2015) (see Figure 6C, D for OPA comparison). LO also exhibited a preponderance of contralaterally centered pRFs (Figure 6E, F). For each participant, region and hemisphere we calculated the position in X corresponding to 50% of the centers in each ROI (cdf = 0.5, inset in Figure 6B, D, and F). We then tested whether these values differed significantly from 0, which

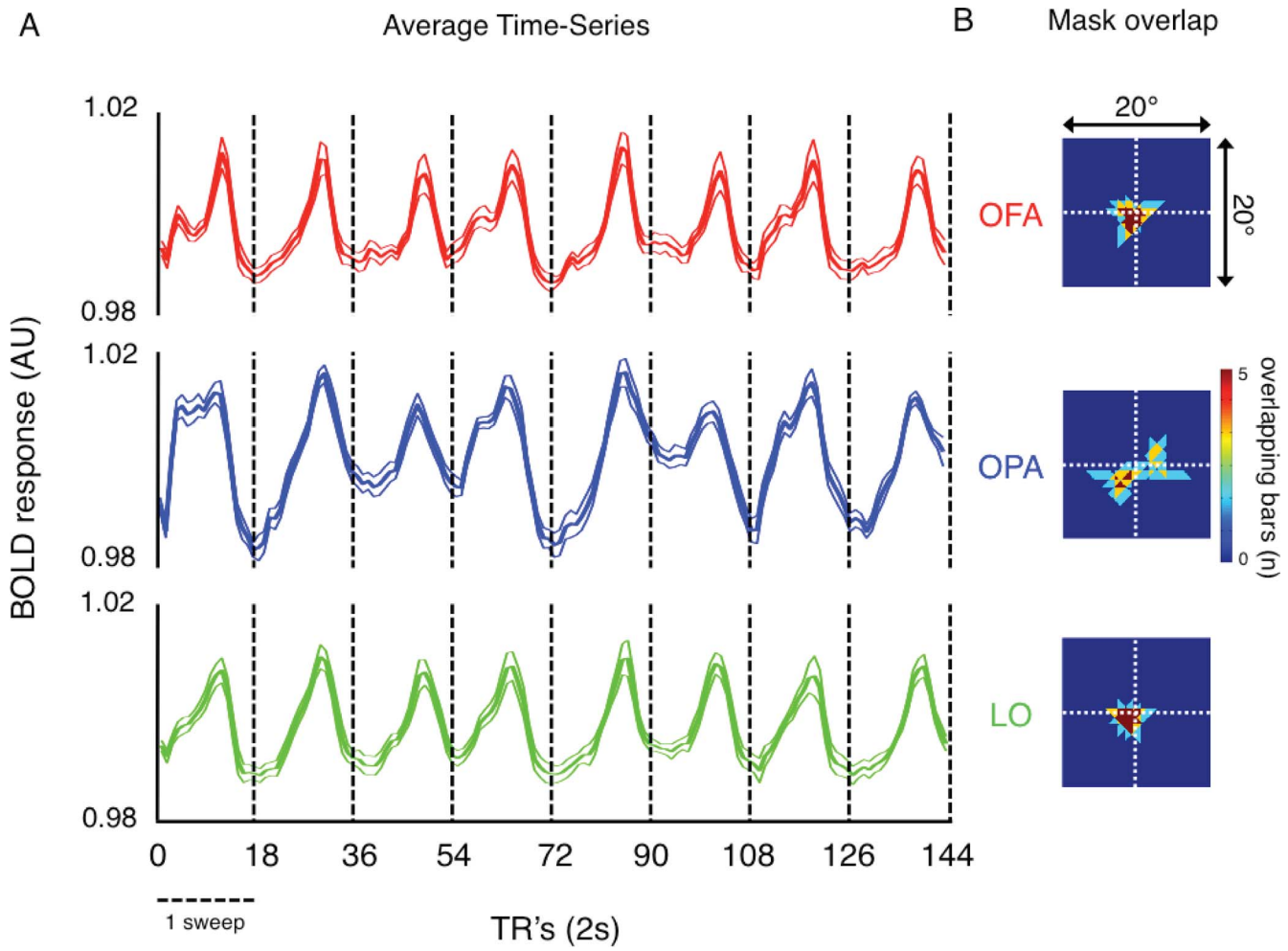

Figure 4. Retinotopic sensitivity in OFA, OPA and LO. (A) The average time-series (± *SEM*) of all voxels in right OFA (red time-series), OPA (blue time-series), and LO (green time-series) averaged across participants ($n = 16$ for OFA and OPA; $n = 8$ for LO) during pRF mapping. These average time-series show clearly eight peaks of activity in all regions. In all regions, each peak occurs once during each of eight sweeps of our mapping stimulus (18 TRs per sweep; vertical dashed black lines denote the start/end of each sweep). The portion of the visual field at which bar positions corresponding to each peak (corrected for the delay in hemodynamic response) overlap is also shown for all regions in (B). In both OFA and LO, the region of maximum overlap occupies a restricted region of the lower left visual field, close to, but importantly left of the vertical meridian. In OPA, the region of maximum overlap occupies a more distributed region of the lower left visual field. These plots represent the portion of the visual field that each area is most sensitive to, respectively.

represents the vertical meridian (*t* test against no contralateral bias assumption). Contralateral biases were significant in all ROIs and hemispheres ($p < 0.05$, in all cases).

Third, we sought to quantify the contralateral lower visual field biases in all ROIs (Silson et al., 2015). We performed the same distribution analysis as above but now for pRF centers in the Y dimension (lower-upper visual field position). Group-averaged distributions (Figure 7A), and CDFs (Figure 7B), quantify the lower visual field bias in both left and right OFA, respectively, with the majority of pRF centers for OFA found to be within the lower visual field (Figure 7B). Again, such a distribution of pRF centers is entirely consistent with the contralateral lower visual field bias reported previously for OPA (Silson et al., 2015) (see Figure 7C, D for OPA comparison) and the contralateral lower visual field biases evidenced in both left and right LO (Figure 7E, F). These distributions were also found to differ significantly from 0 in all regions and hemispheres ($p < 0.02$, in all cases), using the criterion described above.

Finally, we examined the distribution of pRF sizes in left and right OFA, OPA, and LO, respectfully. Here, we calculated the proportion of voxels with pRF sizes ranging from 0°–10° (0.25° bins). Group-averaged pRF size distributions (Figure 8A) and CDFs (Figure 8B), quantify the small pRF size of OFA voxels, relative to

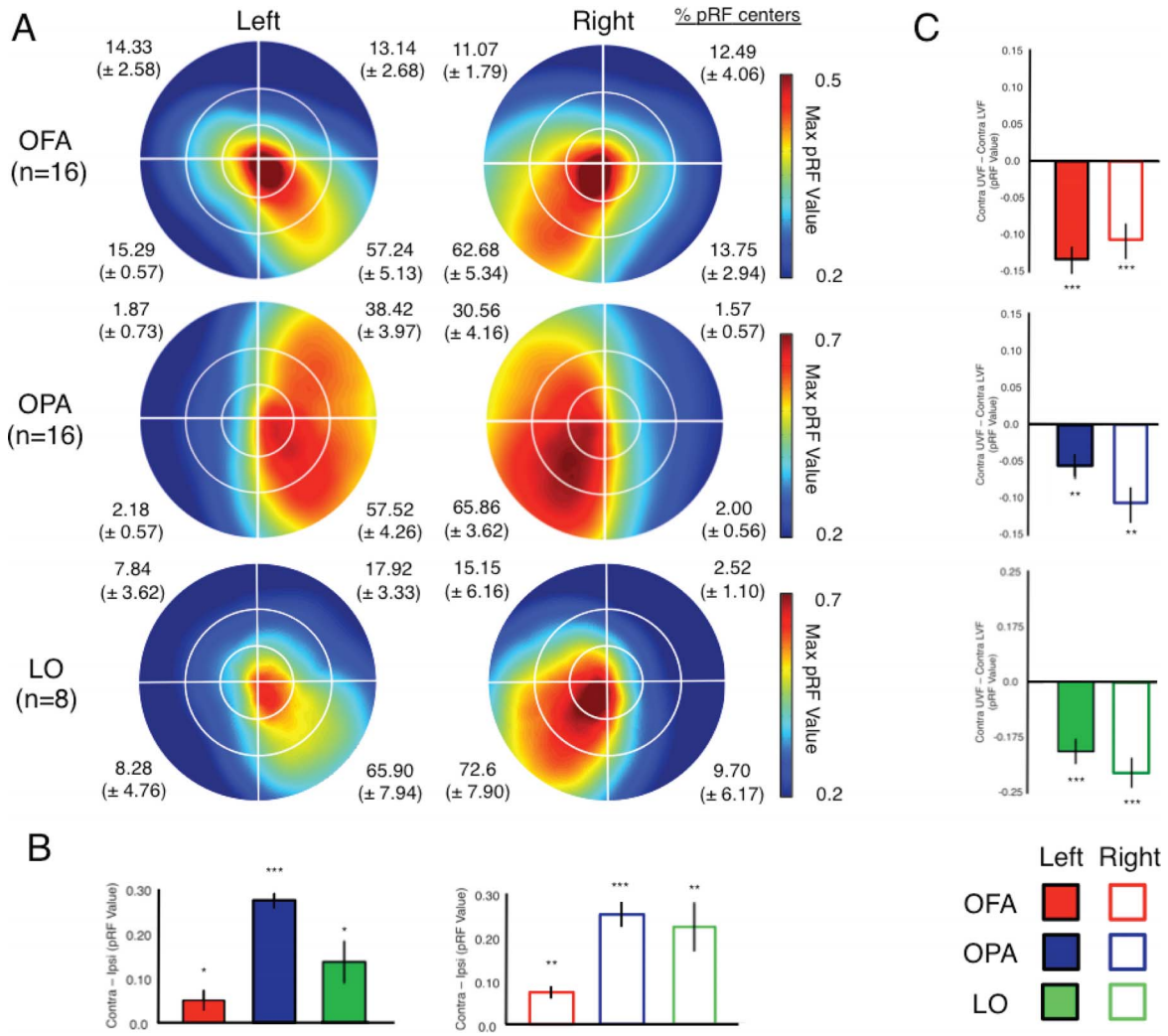

Figure 5. Visual field coverage and visual field biases in left and right OFA, OPA, and LO. (A) Group-average visual field coverage for the left and right OFA are shown **(**top row**)**. Both ROIs exhibit a bias for the contralateral lower visual field, albeit concentrated near fovea within the contralateral field. A similar, but more peripheral bias is evident for left and right OPA (middle row). Similar to OFA, LO also exhibits a foveal yet contralateral visual field bias (bottom row). The more restricted spatial extent of OFA and LO relative to OPA reflects the contralateral yet foveal nature of pRFs in these regions. The percentage of pRF centers (mean ± *SEM*) within each quadrant of the visual field is given for each ROI and confirms the contralateral lower visual field bias in OFA, OPA, and LO, bilaterally. (B) Bars depict the contralateral biases present in left OFA, OPA and LO (left column) and right OFA, OPA and LO, respectively (right column). In all cases, bars depict the mean pRF value in the contralateral *minus* ipsilateral visual fields. Contralateral biases were found to be significant (relative to zero) in all ROIs (*$p < 0.05$, **$p < 0.01$, ***$p < 0.001$), although of note, the contralateral biases present within OFA and LO are markedly weaker than OPA, which again reflects (a) the more foveal nature of OFA and LO RFs and (b) the use of a 2D-Gaussian model of RFs implemented here. (C) Bars depict the elevation bias present within left and right OFA (top), left and right OPA (middle) and left and right LO (bottom), respectively. Bars depict the mean pRF value in the contralateral upper *minus* contralateral lower visual fields. All regions exhibit a significant (relative to zero) contralateral lower visual field bias (**$p <$ 0.01, ***$p < 0.001$).

those in OPA (Figure 8C, D). LO receptive field sizes (Figure 8E, F) were intermediate between the two other ROIs, being both slightly larger than OFA, but also, slightly smaller than OPA. On average, the proportion of OFA pRF sizes peak at ~1.5° and exhibit a fairly rapid decline as pRF sizes increase. In contrast, the distribution of pRF sizes in OPA are more normal, with the proportion of pRF sizes peaking at ~3°. The distribution of pRF sizes in LO are slightly broader than those in OFA, peaking at ~2°, but remain narrower than in OPA. Both OFA and LO pRFs were significantly smaller than those in OPA in both hemispheres (t test of pRF size where cdf = 0.5; $p <$ 0.05, in both hemispheres), with no significant difference in pRF sizes between either OFA and LO or between hemispheres for the same ROI ($p > 0.05$).

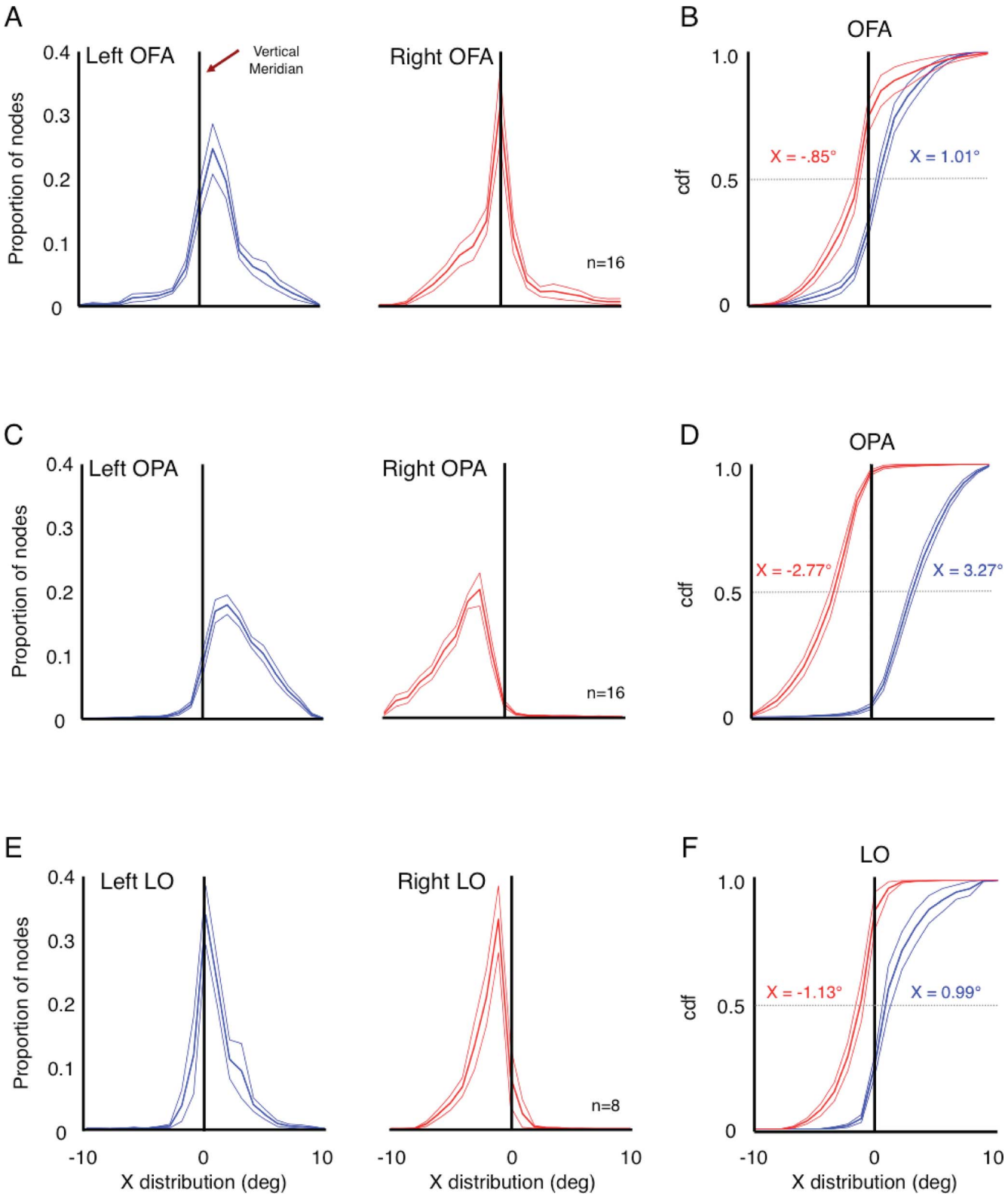

Figure 6. Distribution analyses of pRF properties of left and right OFA, OPA, and LO in the X dimension. (A) Group-average distributions (mean ± *SEM*) of pRF centers in the X dimension (left-right visual field position) for left (blue lines) and right (red lines) OFA. In both cases the majority of the distributions are located to the contralateral side of the vertical meridian (solid black line at X = 0). (B) Cumulative distribution functions (cdf) for pRF centers in the X dimension (same colors as above). The locations in X corresponding to 50% of the voxels (cdf = 0.5—gray dashed line) are inset. In both regions, this median point is located into the

→

←
contralateral visual field. (C) Group-average distributions of pRF centers in the X dimension (left-right visual field position) for left (blue lines) and right (red lines) OPA. Both regions exhibit striking contralateral biases, with the vast majority of each distribution skewed contralaterally. (D) Left and right OPA cdf's for pRFs in the X dimension. RFs in both regions are almost entirely contained within the contralateral visual field. X values inset are as above. (E) Group-average distributions of pRF centers in the X dimension (left-right visual field position) for left (blue lines) and right (red lines) LO. Both regions exhibit contralaterally skewed distributions. (F) Left and right LO cdfs for pRFs in the X dimension. The majority of RFs in both regions are contained within the contralateral visual field. X values inset are as above.

Taken together, our analyses of the pRF properties of these regions reveal a significant contralateral lower visual field bias, coupled with a more concentrated representation of fovea and relatively small receptive field sizes in both OFA and LO, respectively. Notwithstanding differences in pRF size between OFA, LO, and OPA, all regions nevertheless exhibit a consistent and significant bias for the contralateral lower visual field.

How do the biases in OPA, OFA, and LO compare with those within retinotopic maps?

OFA, OPA, and LO, exhibit significant biases for the contralateral lower quadrant of the visual field (bilaterally), but should they be considered quadrant representations? In order to place these retinotopic biases in the context of those present within retinotopically defined maps, some of which explicitly represent a single visual quadrant, we computed initially visual field coverage and visual field biases in all retinotopic maps (Figure 9A), the boundaries of which were defined using independent data acquired using flickering checkerboards (see methods and Figure 9). The representations of the visual field within these maps are entirely consistent with a large number of previous reports (DeYoe et al., 1996; Engel et al., 1994; Larsson & Heeger, 2006; Sereno et al., 1995; Wandell et al., 2007). We compared both contralateral (Figure 9B) and elevation (Figure 9C) biases in all retinotopic and category-selective ROIs. All ROIs exhibited significant contralateral biases. The contralateral bias within OPA was comparable to many retinotopic maps, with V1 exhibiting the largest contralateral bias. Interestingly, the magnitude of the contralateral bias in OFA and LO was similar to both V3d and LO1 and can be attributed to their location, either entirely within, or in close proximity to, the large foveal confluence found near the occipital pole (Figure 1C, D). Such foveal pRF locations would lead to reduced contralateral biases due to the use of the 2D-Guassian pRF model (Dumoulin & Wandell, 2008; Silson et al., 2015) employed here. Considering elevation biases, V1, V3A, and V3B did not exhibit a significant bias to either the upper or lower visual fields—a result entirely consistent with their hemifield representations (Swisher et al., 2007; Wandell et al., 2007). In contrast, all other visual field maps, as well as OPA, OFA, and LO exhibited significant biases for the contralateral lower visual field. In general, the magnitudes of the lower field biases in our category-selective ROIs were smaller than those in V2d and V3d, which have explicit lower quadrant representation.

Retinotopic coding within OFA in the absence of consistently clear retinotopic maps

Consistent with a number of previous reports (Larsson & Heeger, 2006; Sayres & Grill-Spector, 2008; Wandell et al., 2007; Winawer et al., 2010), we do not observe consistently clear progressions of the visual field immediately ventral of our other lateral surface maps, in a region previously referred to as "no man's land" (Winawer et al., 2010). The lack of consistently clear maps in this region has been attributed recently to proximity to distortions in the local magnetic field caused by the dural sinus, termed "venous eclipse" (Winawer et al., 2010). Interestingly, our OFA ROIs were situated generally in close proximity to, albeit slightly superior of, the venous eclipse (Figure S1). Given this proximity, we examined whether distortions of the visual field within OFA caused by this artifact could explain the largely quadrant representations measured therein; the implication being that genuine representations of the upper visual field are potentially being masked or warped spatially by such distortions. We chose to assess this effect by measuring the proportional overlap between OFA and the venous eclipse (see methods and Figure S1). Our analyses highlight that at the group level ~10% of OFA nodes overlap with the venous eclipse, bilaterally, with many participants showing little or no overlap and a small number showing more substantial overlap. The fact that some overlap exists, coupled with the overall proximity of the OFA to the eclipse, means we cannot completely rule out the influence of this artifact on our measurements of the OFA.

Pattern of results not specific to localization method

Finally, in our main analyses, our scene- and face-selective ROIs were defined using an on/off design of

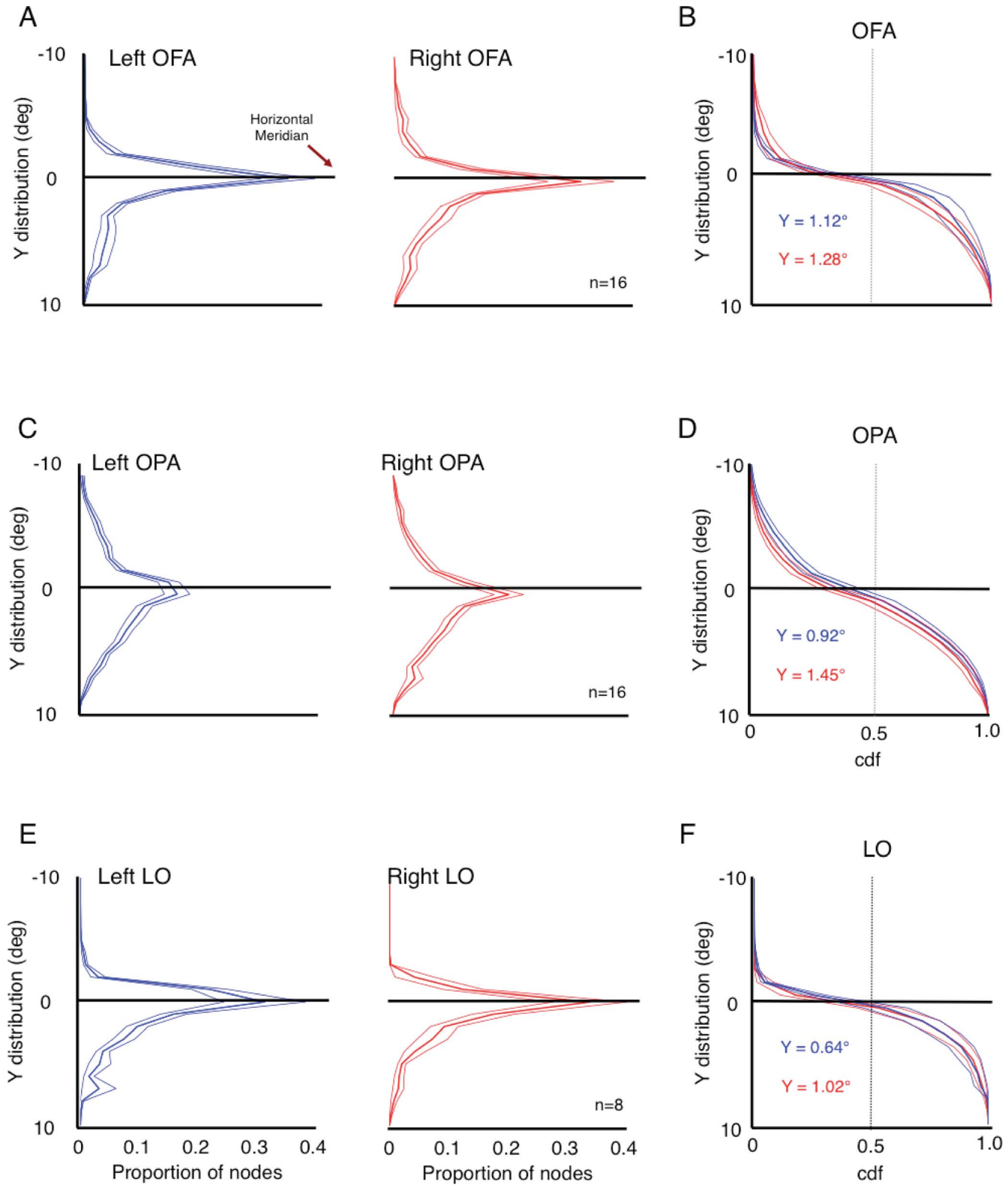

Figure 7. Distribution analyses of pRF properties of left and right OFA, OPA, and LO in the Y dimension. (A) Group-average distributions of pRF centers in the Y dimension (left-right visual field position) for left (blue lines) and right (red lines) OFA. In both regions, more of the distributions are located below the horizontal meridian (solid black line at Y = 0), indicative of a lower visual field bias in both regions. (B) Left and right cdfs of pRFs in the Y dimension are shown for both regions. The locations in Y corresponding to 50% of voxels (cdf = 0.5—gray dashed line) are inset. In both regions, this position is within the lower visual field. (C) Group-average →

←
distributions of pRF centers in the Y dimension are shown for left and right OPA. Both regions exhibit similar biases for the lower visual field. (D) Left and right cdfs for OPA confirm the biases for the lower visual field. Y values inset are as above. (E) Group-average distributions of pRF centers in the Y dimension are shown for left and right LO. Both regions exhibit strong biases for the lower visual field. (F) Left and right cdfs for LO confirm the biases for the lower visual field. Y values inset are as above.

scenes versus faces and vice versa. In a subset of participants ($n = 5$), however, we localized these same ROIs using a multiblocked design to assess the consistency in localization. In each participant we identified the peak voxel of selectivity within OPA and OFA in a number of different ways (e.g., on/off design, blocked Scenes vs. Faces, blocked Scenes vs. Objects or blocked Faces vs. Objects). Notwithstanding subtle displacements in peak voxel location, the peak of selectivity within each ROI was highly reliable across participants and functional contrasts (Figure S2). For instance, irrelevant of the method used to define OFA, the peak voxel was always found to fall outside of our retinotopic definitions across these participants. We are confident, therefore, that our assessments of the relationship each ROI has with underlying retinotopy is not biased by our primary method of localization.

Discussion

We combined detailed mapping of both pRFs and category-selectivity to quantify the spatial relationship between scene-, face-, and object-selective areas of lOTC and the visual field maps that tile this cortical surface. Further, we characterized and compared the pRF profiles of these regions. Our data highlight that whereas OPA overlaps with multiple maps of the visual field, in particular V3B and LO2, LO overlaps two predominantly (LO1 and LO2), and OFA shows a vanishingly small overlap with any maps. Despite this lack of consistent overlap, retinotopically driven responses in OFA are highly reliable, and OFA exhibits a significant contralateral (and foveal) lower visual field bias similar to that observed in OPA and LO (Sayres & Grill-Spector, 2008), reflecting a general contralateral lower field bias across lOTC (Kravitz et al., 2013; Silson et al., 2015).

Correspondence between OPA, OFA, LO, and visual field maps within lOTC

Our analyses of the spatial relationship between OPA and lateral retinotopic maps are, for the most part, consistent with a previous report (Nasr et al., 2011). That is, OPA was found largely anterior of V3A and extended inferiorly from its superior boundary close to V7 (IPS0), through V3B and LO1 (Nasr et al., 2011). Unlike the previous report, we quantified the relationship with underlying retinotopy across a large number of participants and hemispheres and demonstrate that OPA overlaps predominantly with V3B and LO2, relative to other maps, but also extends slightly anteriorly of these regions.

A section of OPA overlapped with regions of cortex anterior of V3B and LO2 and potentially includes TO1 and TO2, which are putative hemifield maps that overlap motion-selective V5/MT (Amano et al., 2009). Here, we were unable to resolve such representations reliably across participants. It is possible therefore that the portion of OPA which lies anterior of V3B and LO2 corresponds to these maps, in particular, the more posterior area TO1 (Amano et al., 2009). Despite not observing clear progressions in the visual field anterior of V3B/LO2, this region nevertheless produced reliable responses to our pRF mapping stimulus. Our pRF characterization of this nonoverlapping region alone demonstrated a contralateral lower visual field bias, similar to that observed for OPA as a whole. Notwithstanding the significant lower field bias within OPA, a more modest representation of the upper visual field is still evident therein. Given that the retinotopic maps directly antecedent to OPA (V2d, V3d, LO1, and LO2) all contain representations restricted largely to the lower quadrant, the upper visual representation in OPA must arise principally via its overlap with V3B, and to a lesser extent V3A and V7—all of which represent a full hemifield (Swisher et al., 2007; Wandell et al., 2007).

In general, OFA exhibited a very small degree of overlap with retinotopically mapped regions of lOTC. OFA was located typically ventral and slightly anterior of the inferior boundaries of our lateral maps. Despite this, we observed highly reliable retinotopically specific responses in OFA, and our analyses of its pRF profile demonstrate clearly that it represents information about visual space retinotopically. These analyses highlight a significant contralateral lower visual field bias within OFA, with more pRF centers within, and more representation of, the contralateral lower quadrant than all other quadrants of the visual field. Additionally, through analyses of pRF distributions we quantified the extent of both the contralateral and lower visual field biases present within OFA. OFA also exhibits a strong preference for the fovea, as evidenced by tight clustering of pRF centers about the vertical meridian, and small receptive fields (relative to OPA).

Although analyzed across fewer participants, LO exhibited the majority of overlap with two visual field

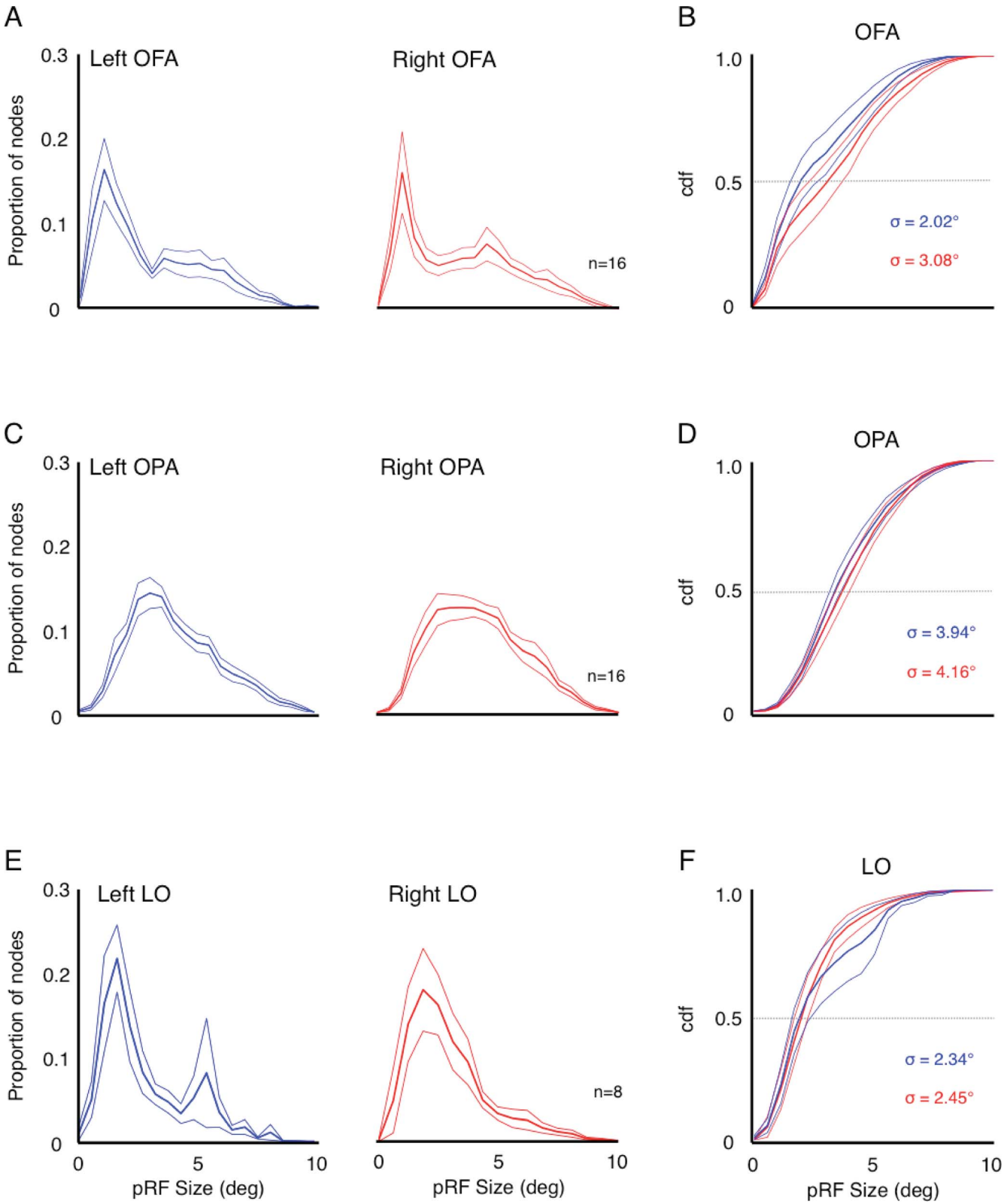

Figure 8. Distribution analyses of pRF sizes of left and right OFA, OPA, and LO. (**A**) Group-average distributions of pRF sizes (sigma) for left (blue lines) and right (red lines) OFA. Both regions exhibit relatively small receptive fields, which peak at ~1.5° in both regions. (B) Left and right pRF size cdfs for OFA, bilaterally. The sizes of pRFs at 50% of the voxels (cdf = 0.5) are inset. (C) Group-average distributions of pRF sizes for left and right OPA. Relative to OFA, both regions exhibit a broader and more even distribution of pRF sizes, which peak at ~3°, twice the size of OFA pRFs. (D) Left and right cdf's for OPA, bilaterally. The pRF sizes inset are as above. (E) →

←

Group-average distributions of pRF sizes for left and right LO. LO pRFs are similar in size, if not slightly larger than those in OFA, peaking ~2.0°, but remain smaller than those in OPA. (F) Left and right cdfs for LO, bilaterally. The pRF sizes inset are as above.

maps (LO1 and LO2), a feature highlighted previously (Larsson & Heeger, 2006; Sayres & Grill-Spector, 2008). As a whole, similar to OFA and OPA, LO exhibited a significant bias for the contralateral lower visual field (Figure 5). Given the overlap with LO1 and LO2, both of which exhibit largely lower quadrant representations (Figure 9), such a retinotopic profile is predicted. The foveal location and small size of LO receptive fields, relative to OPA, make its profile more similar to that exhibited by OFA and likely reflects their shared proximity to the foveal confluence (Figure 1B).

What are the implications of the spatial relationship to underlying retinotopy?

Our data highlight a contrasting relationship between OPA, OFA, LO and retinotopic maps within lOTC. OPA and LO both overlap multiple maps, whereas OFA overlapped almost none. What are the implications for such differing relationships to underlying retinotopy? The fact that OPA encompasses multiple maps of the visual field calls into question whether researchers should continue to conceptualize it as a single scene-selective region. Scenes are a heterogeneous category of stimuli and it is possible that multiple visual features, which drive scene-selectivity, are represented across multiple maps. That is, perhaps OPA is made up of a cluster of visual areas (*maps*), each one with the potential of performing a number of related but different visual computations, a concept in line with the visual field map clusters model proposed by Wandell, Brewer, and Dougherty (2005). Expanding this interpretation further, our measurements of the visual field coverage within V3B and LO2 (maps exhibiting highest degree of overlap with OPA) demonstrate that whereas V3B represents the entire contralateral visual field, LO2 largely represents the contralateral lower quadrant. Such differential representation of visual space raises the possibility that these two visual field maps undertake quite different visual computations that relate to the types of visual features found typically at those locations within scenes.

In the case of LO, which overlaps maximally with LO1 and LO2, previous neuroimaging work (Larsson & Heeger, 2006; Larsson, Landy, & Heeger, 2006) demonstrated differential sensitivity to low-level visual features within these maps. Further, neurostimulation studies (Silson et al., 2013) demonstrated a double dissociation between LO1 and LO2. Specifically, disruption to LO1, but not LO2, significantly perturbed orientation discrimination, whereas disruption to LO2, but not LO1, significantly disturbed shape (curvature) discrimination (Silson et al., 2013). To the extent that similar dissociations of function exist for other retinotopic maps, it is possible, therefore, that similarly distinct mechanisms could be present within the functionally defined OPA.

In contrast, the lack of any consistent overlap between OFA and retinotopic maps suggests the same logic cannot be applied there, and perhaps OFA should be considered as a uniform area that contains an underlying retinotopic organization. Unlike scenes and objects, faces are a more homogenous category of stimuli with less variation in visual features and so perhaps the visual features driving face-selectivity are capable of being represented within a single region. However, there are two key factors that may also contribute to the pattern of results we observed. First, the lack of consistently clear retinotopic maps within OFA may also reflect our currently limited ability to clearly resolve polar angle maps within foveally-biased cortex (Schira et al., 2009; Winawer et al., 2010) using the pRF methods employed here. A very recent study, however, employing a face-specific variant of pRF mapping (Kay et al., 2015) demonstrated a contralateral and lower bias in OFA (referred to as IOG in Kay et al., 2015) consistent with the data reported here. Second, in certain individuals, representations of the visual field in this region of lOTC may be distorted due to scanner artifacts introduced by the vasculature of the individual. Our analyses show there is minimal overlap between the venous eclipse and OFA, but distortions produced by this artifact may still be influencing our results. Thus, although our data suggest that OFA remains spatially separate from lOTC visual field maps, this does not exclude the possibility that, with improved mapping paradigms, overlapping retinotopic maps will be identified in this region.

Implications for scene, face, and object processing

The retinotopic biases observed here have important implications both theoretically, in terms of the types of visual computations that may be performed by these areas, and practically, in terms of neurostimulation studies of these regions.

First, the fact that OFA represents predominantly the contralateral lower visual field suggests a potentially more restrictive role in face processing than has been proposed previously (Haxby et al., 2000). OFA has been implicated as the first area in a series of core face processing units

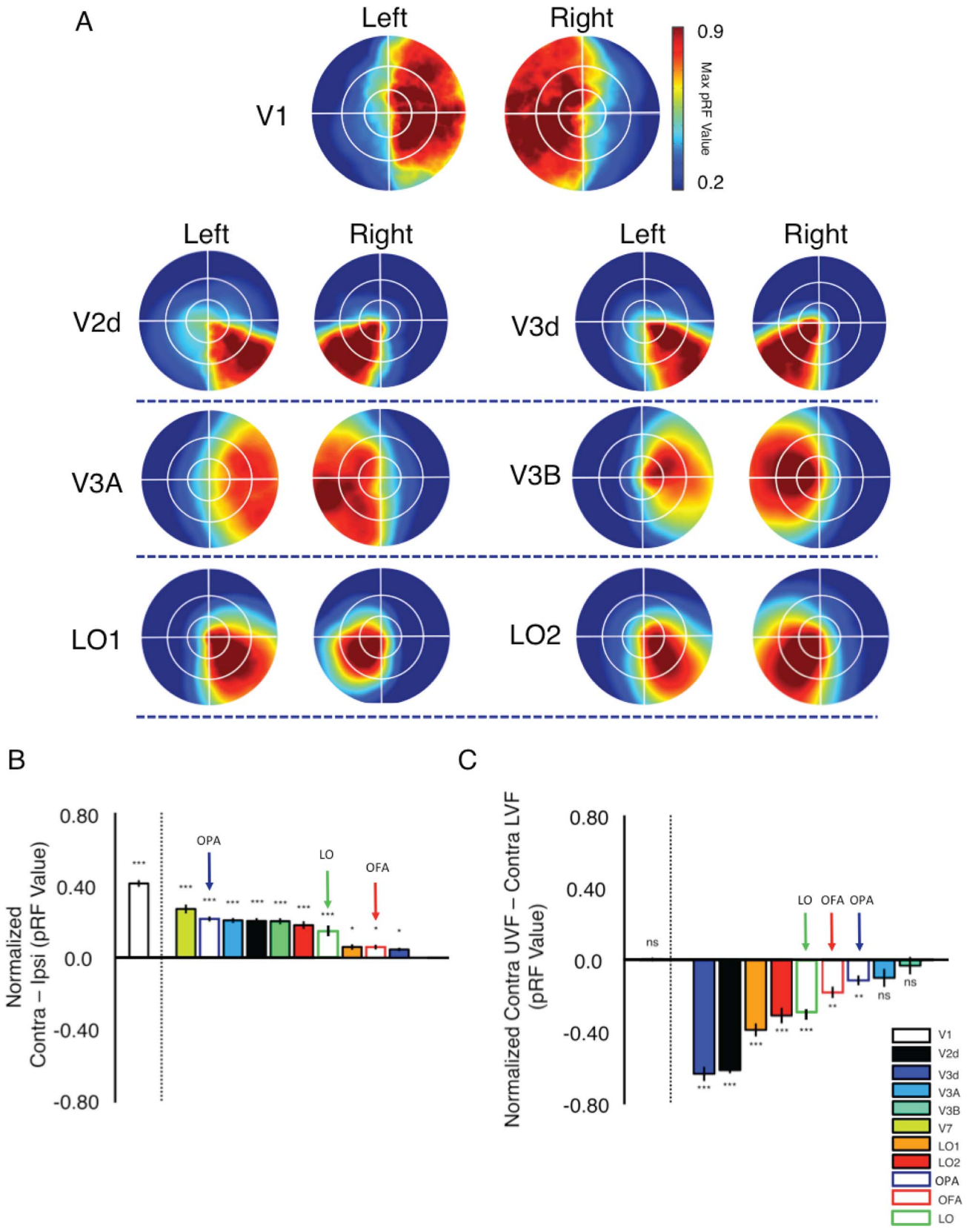

Figure 9. Visual field coverage and retinotopic biases within all retinotopic maps and category-selective ROIs. (A) Group-average ($n = 7$) visual field coverage plots of our retinotopic maps are shown for both left and right hemispheres. For this analysis visual field map boundaries were defined on the basis of checkerboard mapping data and then applied to our primary mapping data. Consistent with

→

←

a large number of previous reports, V1, V3A, and V3B contain full hemifield representations of the contralateral visual field, whereas V2d and V3d represent the contralateral lower quadrant only. Whether or not LO1 and LO2 represent a full hemifield or single quadrant is debated. Our measurements suggest largely quadrant representations within these maps. (B) Bars depict the contralateral bias present within all retinotopic and category-selective ROIs ordered in descending order of bias magnitude. All ROIs exhibit a significant bias (relative to zero) for the contralateral visual field. The magnitude of this bias in OFA was comparable to both LO1 and V3d and is attributable to their proximity to the large foveal confluence in both hemispheres. (C) Bars depict the elevation bias in all ROIs, ordered in descending order of magnitude, with V1 separate (dashed vertical line separates V1). All ROIs exhibit a significant contralateral lower visual field bias (relative to zero) except V1, V3A, and V3B, which was predicted given the full hemifield representations therein (*$p < 0.05$, **$p < 0.01$, ***$p < 0.001$).

throughout human OTC. Indeed, it was originally hypothesized that the OFA not only projected to, but also, received information from both the more anterior and dorsal superior temporal sulcus, STS, and more anterior and ventral fusiform face area, FFA (Haxby et al., 2000; Kanwisher et al., 1997). Our analyses suggest that OFA is likely to exhibit a preference for facial visual features that typically occur below the point of fixation and may also exhibit a preference for the correct contralateral configuration of such features. Such a preference for contralaterally preserved configurations has been demonstrated within body-selective EBA (Chan, Kravitz, Truong, Arizpe, & Baker, 2010) and is consistent with a very recent report of a face-based topographic representation (termed faciotopy) within OFA (Henriksson, Mur, & Kriegeskorte, 2015). Further, recent evidence suggests that the function of ventral FFA remains largely intact following surgical resection of lateral regions of OTC, which include OFA (Weiner, 2015). This apparent independence of OFA and FFA is consistent with the idea of differential representations of space within OFA (contralateral lower) reported here, and FFA (contralateral upper), suggested previously (Kravitz et al., 2013; Silson et al., 2015). Further, a lower visual field advantage for objects has been demonstrated previously (Sayres & Grill-Spector, 2008) and is consistent with the magnitude of the elevation bias reported here for LO.

Second, differential sensitivity for the lower over the upper field within OPA, OFA, and LO suggests that when stimulated with transcranial magnetic stimulation (TMS), differential effects on behavior may be observed as a function of stimulus position in the visual field. Historically, TMS experiments investigating category-selectivity have presented stimuli at fixation and applied TMS to a lateralized target (typically the peak voxel of selectivity within the ROI), often demonstrating a deficit in the discrimination or recognition of the targeted regions preferred category (Dilks et al., 2013; Pitcher et al., 2007; Pitcher et al., 2009; Pitcher et al., 2011). OPA, OFA, and LO all contain pRFs that overlap fovea and such foveal representations likely account for the behavioral deficits reported despite lateralized stimulation. Our data suggest that these effects could potentially be amplified if stimuli were placed in the location of the visual field most represented by these regions (i.e., contralateral lower visual field). Indeed, previous neurostimulation work utilizing contralaterally presented stimuli have been successful in the LO regions LO1 and LO2 (Silson et al., 2013). Understanding where the peak-voxel falls with respect to underlying retinotopy will be particularly important for OPA. Our observations suggest that V3B contains a representation of the upper visual field that is not shared by LO2. If the target voxel for TMS were therefore within the upper field representation of V3B in one participant and the lower field representation of LO2 in another, effects of TMS may interact and be influenced by the portion of the visual field represented by the retinotopic map encompassing the peak-voxel.

Given the prominent and pervasive role of retinotopy throughout OTC demonstrated by us and many others (Amano et al., 2009; Golomb & Kanwisher, 2012; Hasson et al., 2003; Kravitz et al., 2010; Kravitz et al., 2013; Larsson & Heeger, 2006; Levy, Hasson, Avidan, Hendler, & Malach, 2001; Sayres & Grill-Spector, 2008; Schwarzlose et al., 2008; Silson et al., 2013; Silson et al., 2015; Wandell et al., 2007), understanding the complex relationship a targeted category-selective region has with the underlying retinotopy is essential. It also raises the question of whether these regions should be considered as truly category-selective. If OPA is comprised of multiple retinotopic subdivisions that operate potentially independently, then labeling the whole region as scene-selective, based on its overall greater response to scenes relative to faces (or another stimulus category) in a univariate contrast, may be overly simplistic. More sophisticated imaging and analysis paradigms (e.g., event-related fMRI, multi-vovel pattern analysis [MVPA]), which take into account the statistics of the images being presented (Groen, Ghebreab, Prins, Lamme, & Scholte, 2013; Watson, Young, & Andrews, 2016), may allow us to more clearly define the response profiles of these regions, as a whole, and identify potential differences (if any) in response profiles specific to a regions subdivisions (Silson et al., 2013).

Contralateral lower field biases throughout lOTC

Notwithstanding differences in relationship to underlying retinotopic maps, receptive field size and extent of visual field coverage between OPA, OFA, and LO, all areas exhibit similar retinotopic bias profiles, with a significant overrepresentation of the contralateral lower visual field. Coupled with previous work demonstrating a lower visual field bias in EBA (Chan et al., 2011; Schwarzlose et al., 2008), there is now an emerging literature of contralateral lower visual field biases across much of lOTC (Kravitz et al., 2013; Silson et al., 2015). Such biases mirror the explicit segregation of the visual field in antecedent dorsal early visual cortex and offer a plausible organizational framework for the development of category-selectivity throughout lOTC, whereby category-selective regions are constrained functionally by the underlying retinotopic organization of the area of cortex they colocalize with. From such a mechanism, it follows that the ventral surface of OTC should exhibit the opposite bias (contralateral upper visual field), and there is evidence to suggest this is indeed the case for ventral scene- (Silson et al., 2015) and object- (Kravitz et al., 2010), and to a lesser extent face-selective areas (Silson et al., 2015).

Conclusion

Here we quantified across a large number of hemispheres the spatial relationship between scene-, face-, and object-selective regions of lOTC and the visual field maps that tile this cortical surface. We show that OPA overlaps multiple maps of the visual field, LO overlaps LO1 and LO2, and OFA exhibits almost no overlap with any retinotopically-defined maps. The multiple maps that overlap OPA suggest it is likely not appropriate to think of it as a single region, whereas the lack of any consistent map overlapping OFA suggests a different principle may dominate its organization. Despite differences in overlap patterns, all regions exhibit strongly retinotopic voxels and demonstrate significant biases for the contralateral lower quadrant of the visual field. Throughout lOTC, there appears no simple consistent spatial relationship between category-selective regions and the visual field maps that tile its surface. Characterizing the relationship between retinotopy and category-selective regions of OTC remains an important step in order to better understand the complex interactions between cortical regions that underpin human visual processing.

Keywords: retinotopy, category-selectivity, population receptive fields

Acknowledgments

This work was supported by the Intramural Research Program of the National Institute of Mental Health (MH002909-08).

Commercial relationships: none.
Corresponding author: Edward H. Silson.
Email: ed.silson@nih.gov.
Address: Laboratory of Brain and Cognition, National Institute of Mental Health, National Institutes of Health, Bethesda, MD, USA.

References

Amano, K., Wandell, B. A., & Dumoulin, S. O. (2009). Visual field maps, population receptive field sizes, and visual field coverage in the human MT+ complex. *Journal of Neurophysiology*, *102*(5), 2704–2718, doi:10.1152/jn.00102.2009.

Bettencourt, K. C., & Xu, Y. (2012). The Role of Transverse Occipital Sulcus in Scene Perception and Its Relationship to Object Individuation in Inferior Intraparietal Sulcus, *Journal of Cognitive Neuroscience, 25*(10), 1711–1722.,doi:10.1162/jocn.

Chan, A. W.-Y., Kravitz, D. J., Truong, S., Arizpe, J., & Baker, C. I. (2010). Cortical representations of bodies and faces are strongest in commonly experienced configurations. *Nature Neuroscience*, *13*(4), 417–418, doi:10.1038/nn.2502.

Cox, R. W. (1996). AFNI: Software for Analysis and Visualization of Functional Magnetic Resonance Neuroimages, *Computers and Biomedical Research, 27*(3),162–173.

DeYoe, E. A., Carmant, G. J., Bandettini, P., Glickman, S., Wieser, J. O. N., Cox, R., & Neitz, J. A. Y. (1996). Mapping striate and extrastriate visual cerebral cortex human. *Proceedings of the National Academy of Sciences, USA, 93*, 2382–2386.

Dilks, D. D., Julian, J. B., Paunov, A. M., & Kanwisher, N. (2013). The occipital place area is causally and selectively involved in scene perception. *The Journal of Neuroscience: the Official Journal of the Society for Neuroscience*, *33*(4), 1331–1336a, doi:10.1523/JNEUROSCI.4081-12.2013.

Downing, P. E., Jiang, Y., Shuman, M., & Kanwisher, N. (2001). A Cortical Area Selective for Visual Processing of the Human Body. *Science*, *293*(5539), 2470–2473.

Dumoulin, S. O., & Wandell, B. A. (2008). Population

receptive field estimates in human visual cortex. *NeuroImage*, *39*(2), 647–660.

Engel, S. A., Rumelhart, D. E., Wandell, B. A., Lee, A. T., Glover, G. H., Chichilinisky, E. J., & Shadlen, M. N. (1994). fMRI of human visual cortex. *Nature*, *369*(6481), 525.

Epstein, R., & Kanwisher, N. (1998). A cortical representation of the local visual environment. *Nature*, *392*, 6–9.

Ferri, F., Chiarelli, A. M., Merla, A., Gallese, V., & Costantini, M. (2013). The body beyond the body: Expectation of a sensory event is enough to induce ownership over a fake hand. *Proceedings of the Royal Society B: Biological Sciences, 280*(1765) 20131140.

Golomb, J. D., & Kanwisher, N. (2012). Higher level visual cortex represents retinotopic, not spatiotopic, object location. *Cerebral Cortex*, *22*(12), 2794–2810, doi:10.1093/cercor/bhr357.

Groen, I. I. A., Ghebreab, S., Prins, H., Lamme, V. A. F., & Scholte, H. S. (2013). From image statistics to scene gist: Evoked neural activity reveals transition from low-level natural image structure to scene category. *Journal of Neuroscience*, *33*(48), 18814–18824.

Hasson, U., Harel, M., Levy, I., & Malach, R. (2003). Large-scale mirror-symmetry organization of human occipito-temporal object areas. *Neuron*, *37*(6), 1027–1041. Retrieved from http://www.ncbi.nlm.nih.gov/pubmed/12670430

Haxby, J. V., Hoffman, E. A., & Gobbini, M. I. (2000). The distributed human neural system for face perception, *Trends in Cognitive Sciences*, *4*(6), 223–233.

Hemond, C. C., Kanwisher, N. G., & De Beeck, H. P. O. (2007). A preference for contralateral stimuli in human object- and face-selective cortex. *PLoS One*, *2*(6), e574.

Henriksson, L., Mur, M., & Kriegeskorte, N. (2015). Faciotopy—A face-feature map with face-like topology in the human occipital face area. *Cortex; a Journal Devoted to the Study of the Nervous System and Behavior*, *72*, 156–167, doi:10.1016/j.cortex.2015.06.030.

Kanwisher, N., McDermott, J., & Chun, M. M. (1997). The Fusiform Face Area: A Module in Human Extrastriate Cortex Specialized for Face Perception. *The Journal of Neuroscience*, *17*(11), 4302–4311.

Kay, K. N., Weiner, K. S., & Grill-Spector, K. (2015). Attention reduces spatial uncertainty in human ventral temporal cortex. *Current Biology*, *25*(5), 595–600.

Kravitz, D. J., Kriegeskorte, N., & Baker, C. I. (2010). High-level visual object representations are constrained by position. *Cerebral Cortex*, *20*(12), 2916–2925, doi:10.1093/cercor/bhq042.

Kravitz, D. J., Peng, C. S., & Baker, C. I. (2011). Real-world scene representations in high-level visual cortex: it's the spaces more than the places. *The Journal of Neuroscience*, *31*(20), 7322–7333.

Kravitz, D. J., Saleem, K. S., Baker, C. I., Ungerleider, L. G., & Mishkin, M. (2013). The ventral visual pathway: Ann expanded neural framework for the processing of object quality. *Trends in Cognitive Sciences*, *17*(1), 26–49, doi:10.1016/j.tics.2012.10.011.

Kravitz, D. J., Vinson, L. D., & Baker, C. I. (2008). How position dependent is visual object recognition? *Trends in Cognitive Sciences*, *12*(3), 114–122, doi:10.1016/j.tics.2007.12.006.

Larsson, J., & Heeger, D. J. (2006). Two retinotopic visual areas in human lateral occipital cortex. *The Journal of Neuroscience*, *26*(51), 13128–13142, doi:10.1523/JNEUROSCI.1657-06.2006.

Larsson, J., Landy, M. S., & Heeger, D. J. (2006). Orientation-selective adaptation to first- and second-order patterns in human visual cortex. *Journal of Neurophysiology*, *95*(2), 862–881, doi:10.1152/jn.00668.2005.

Levy, I., Hasson, U., Avidan, G., Hendler, T., & Malach, R. (2001). Center-periphery organization of human object areas, *Nature Neuroscience*, *4*(5), 533–539.

Malach, R., Reppas, J. B., Benson, R. R., Kwong, K. K., Jlang, H., Kennedy, W. A., & Tootell, R. B. H. (1995). Object-related activity revealed by functional magnetic resonance imaging in human occipital cortex. *Proceedings of the National Academy of Sciences, USA*, *92*(18), 8135–8139.

Nakamura, K., Kawashima, R., Sato, N., Nakamura, A., Sugiura, M., Kato, T., ...Zilles, K. (2000). Functional delineation of the human occipito-temporal areas related to face and scene processing. *Brain*, *123*(9), 1903–1912.

Nasr, S., Liu, N., Devaney, K. J., Yue, X., Rajimehr, R., Ungerleider, L. G., & Tootell, R. B. H. (2011). Scene-selective cortical regions in human and nonhuman primates. *The Journal of Neuroscience*, *31*(39), 13771–13785, doi:10.1523/JNEUROSCI.2792-11.2011.

Niemeier, M., Goltz, H. C., Kuchinad, A., Tweed, D. B., & Vilis, T. (2005). A contralateral preference in the lateral occipital area: sensory and attentional mechanisms. *Cerebral Cortex*, *15*(3), 325–331.

Pitcher, D., Charles, L., Devlin, J. T., Walsh, V., & Duchaine, B. (2009). Triple dissociation of faces,

bodies, and objects in extrastriate cortex. *Current Biology*, *19*(4), 319–324, doi:10.1016/j.cub.2009.01.007.

Pitcher, D., Walsh, V., & Duchaine, B. (2011). The role of the occipital face area in the cortical face perception network. *Experimental Brain Research*, *209*(4), 481–493, doi:10.1007/s00221-011-2579-1.

Pitcher, D., Walsh, V., Yovel, G., & Duchaine, B. (2007). TMS evidence for the involvement of the right occipital face area in early face processing. *Current Biology*, *17*(18), 1568–1573.

Sayres, R., & Grill-Spector, K. (2008). Relating retinotopic and object-selective responses in human lateral occipital cortex. *Journal of Neurophysiology*, *100*(1), 249–267, doi:10.1152/jn.01383.2007.

Schira, M. M., Tyler, C. W., Breakspear, M., & Spehar, B. (2009). The foveal confluence in human visual cortex. *The Journal of Neuroscience*, *29*(28), 9050–9058.

Schwarzlose, R. F., Swisher, J. D., Dang, S., & Kanwisher, N. (2008). The distribution of category and location information across object-selective regions in human visual cortex. *Proceedings of the National Academy of Sciences*, *105*(11), 4447–4452.

Sereno, M., Dale, A. M., Reppas, J. B., Kwong, K. K., Belliveau, J. W., Brady, T. J., & Tootell, R. B. H. (1995). Borders of multiple visual areas in humans revealed by functional magnetic resonance imaging. *Science, 268*(5212), 889–893.

Silson, E. H., Chan, A. W.-Y., Reynolds, R. C., Kravitz, D. J., & Baker, C. I. (2015). A retinotopic basis for the division of high-level scene processing between lateral and ventral human occipitotemporal cortex. *Journal of Neuroscience*, *35*(34), 11921–11935, doi:10.1523/JNEUROSCI.0137-15.2015.

Silson, E. H., McKeefry, D. J., Rodgers, J., Gouws, A. D., Hymers, M., & Morland, A. B. (2013). Specialized and independent processing of orientation and shape in visual field maps LO1 and LO2. *Nature Neuroscience*, *16*(3), 267–269, doi:10.1038/nn.3327.

Silvanto, J., Schwarzkopf, D. S., Gilaie-Dotan, S., & Rees, G. (2010). Differing causal roles for lateral occipital cortex and occipital face area in invariant shape recognition. *The European Journal of Neuroscience*, *32*(1), 165–171, doi:10.1111/j.1460-9568.2010.07278.x.

Swisher, J. D., Halko, M. A., Merabet, L. B., McMains, S. A., & Somers, D. C. (2007). Visual topography of human intraparietal sulcus. *Journal of Neuroscience*, *27*, 5326–5337.

Taylor, J. C., Wiggett, A. J., & Downing, P. E. (2007). Functional MRI analysis of body and body part representations in the extrastriate and fusiform body areas. *Journal of Neurophysiology*, *98*(3), 1626–1633.

Wandell, B. A., Brewer, A. A., & Dougherty, R. F. (2005). Visual field map clusters in human cortex. *Philosophical Transactions of the Royal Society of London. Series B, Biological Sciences*, *360*(1456), 693–707, doi:10.1098/rstb.2005.1628

Wandell, B. A., Dumoulin, S. O., & Brewer, A. A. (2007). Visual field maps in human cortex. *Neuron*, *56*(2), 366–383, doi:10.1016/j.neuron.2007.10.012.

Watson, D. M., Young, A. W., & Andrews, T. J. (2016). Spatial properties of objects predict patterns of neural response in the ventral visual pathway. *NeuroImage*, *126*, 173–183.

Weiner, K. S. (2015). The human face processing network is resilient after resection of specialized cortical inputs. *Journal of Vision*, *15*(12): 1411, doi: 10.1167/15.12.1411. [Abstract]

Weiner, K. S., & Grill-Spector, K. (2011). NeuroImage Not one extrastriate body area: Using anatomical landmarks, hMT +, and visual field maps to parcellate limb-selective activations in human lateral occipitotemporal cortex. *NeuroImage*, *56*(4), 2183–2199, doi:10.1016/j.neuroimage.2011.03.041.

Winawer, J., Horiguchi, H., Sayres, R. A., Amano, K., & Wandell, B. A. (2010). Mapping hV4 and ventral occipital cortex: the venous eclipse. *Journal of Vision*, *10*(5):1, 1–22, doi:10.1167/10.5.1. [PubMed] [Article]

Zeki, S., Watson, J. D., Lueck, C. J., Friston, K. J., Kennard, C., & Frackowiak, R. S. (1991). A direct demonstration of functional specialization in human visual cortex. *Journal of Neuroscience*, *11*(3), 641–649.